Breakup of Thin Liquid Films: From Stochastic to Deterministic

Emmanouil Chatzigiannakis and Jan Vermant*
Department of Materials, ETH Zürich, Vladimir Prelog Weg 5, 8032 Zürich, Switzerland

(Received 5 May 2020; accepted 8 September 2020; published 7 October 2020)

The thinning and rupture of thin liquid films is a ubiquitous process, controlling the lifetime of bubbles, antibubbles, and droplets. A better understanding of rupture is important for controlling and modeling the stability of multiphase products. Yet literature reports that film breakup can be either stochastic or deterministic. Here, we employ a modified thin film balance to vary the ratio of hydrodynamic to capillary stresses and its role on the dynamics of thin liquid films of polymer solutions with adequate viscosities. Varying the pressure drop across planar films allows us to control the ratio of the two competing timescales, i.e., a controlled hydrodynamic drainage time and a timescale related to fluctuations. The thickness fluctuations are visualized and quantified, and their characteristics are for the first time directly measured experimentally for varying strengths of the flow inside the film. We show how the criteria for rupture depend on the hydrodynamic conditions, changing from stochastic to deterministic as the hydrodynamic forces inside the film damp the fluctuations.

DOI: 10.1103/PhysRevLett.125.158001

A fundamental process governing the stability of foams and emulsions is coalescence, which involves the thinning and rupture of the thin liquid films separating two droplets or bubbles [1]. Film drainage is governed by hydrodynamic forces and is well described by deterministic continuum mechanical models [1,2], the simplest one being the generalized Stefan-Reynolds (SR) equation [3], albeit valid only for flat films of constant radius:

$$-\frac{dh}{dt} = \frac{8h^3(P_H - \Pi_{\mathrm{vdW}})}{3\eta_{\mathrm{eff}}R^2} \tag{1}$$

where R is the film's radius, P_H is the hydrodynamic pressure, Π_{vdW} is the disjoining pressure due to the van der Waals (vdW) interactions, h is the thickness, and η_{eff} is an effective viscosity equal to $\eta_{\mathrm{eff}} = n^2\eta$, n is a mobility factor that describes the ability of the interface to carry stress, up to a no slip-boundary condition ($0 < n \leq 2$), and η is the bulk viscosity. More complex models are available for nonplanar films [1], but the simple SR equation captures that the thickness reduction for a given fluid is driven by the pressure drop across the film.

The second process, film rupture, is more complicated. For a nondraining film, Sheludko [4,5] and Vrij [6] showed how fluctuations in thickness, either due to thermal or mechanical perturbations, lead to two opposing effects. The increase of area and curvature leads to a decrease in the local capillary pressure, while the changes in the local thickness affect the Π_{vdW}. This balance results in a critical wavelength $\Lambda_{c,V}$ that cannot be damped by capillarity [6], equal to $\Lambda_{c,V} = \beta h^2\sqrt{\sigma/A_H}$, where σ is the surface tension, β is a constant, and A_H is the Hamaker constant. This wavelength controls the critical thickness h_c at which the film ruptures which is typically several 10 nm [7], much higher than the range of the vdW forces of individual molecules. The direct experimental observation of such capillary waves causing coalescence came forty years later, when Aarts *et al.* [8] used confocal microscopy to study the fluid-fluid interface of a phase-separated colloid-polymer dispersion.

Under dynamic conditions, the lifetime of draining films depends on the competition between the timescales of drainage and rupture [6,9–12]. Coalescence is hence expected to be stochastic in nature. Interestingly, literature reports differ even qualitatively on this point. Some studies clearly confirm this [13–15], while others report a purely deterministic nature [16–18]. In this respect, hydrodynamic stresses couple to capillarity too, and a signature "dimple" can develop in the films, with their thickness being smaller near their edge [19]. The critical thickness is reached earlier at this thinner region, with fluctuations having less time to develop. Recent simulations accounted for this effect by coupling a Gaussian noise to the thinning dynamics [20], predicting a reduction in the standard deviation of the coalescence time as drainage gets faster. However, such approaches cannot explain either the deterministic rupture of stress-free films, which remain flat regardless of the drainage intensity [21–23], or the strongly stochastic rupture of different dimpled films [15,24,25]. Moreover, the underlying assumption of constant critical thickness seems at odds with most literature reports [26–31]. Overall, a closer look into the coupling between capillary, hydrodynamic, and vdW forces seems warranted.

In this Letter, we use a modified thin film balance (TFB) [32] to study the drainage and rupture of both flat and dimpled films for a wide range of hydrodynamic

conditions. By increasing the pressure drop that causes drainage, the relative timescales are varied, seamlessly bridging conditions for slow, quasistatic, drainage regimes with hydrodynamically dominated ones. Moreover, by using solutions of polyisobutylene-in-hexadecane of various concentrations and viscosities, we avoided the effects of inertia and surface stresses, and specifically interrogated the interplay between the observed fluctuations and the applied hydrodynamic forces. We show that film breakup can appear as stochastic or deterministic depending on the capillary number, which characterizes the ratio of hydrodynamic to capillary stresses.

The TFB consists of a fixed-stage microscope (Nikon Eclipse FN1/10 × LWD objective) with a 16-bit gray-scale Hamamatsu ORCA-Flash4.0 CMOS camera (10 ms maximum temporal resolution) for measuring film thickness by interferometry, and a sealed chamber, where the bike-wheel microfluidic device [32] is placed. The pressure of the air inside the chamber is controlled by an Elveflow MK3$^+$ piezoelectric pressure controller. A monochromatic wavelength of 508 nm was used for reflection. Sheludko's interferometry method [5] allows a thickness resolution of ≃2 nm. Images were analyzed with ImageJ and MATLAB. Evaporation was prevented by adding solvent in the chamber.

Initially, a thick film was created and its point of mechanical equilibrium was determined by applying an extra pressure in the air side P_i, equal to $P_i = -2\sigma/R_{bw} + P_\infty$, where the second term is the Laplace pressure due to the curvature of the Plateau border, with R_{bw} being the radius of the cell's hole, and P_∞ is the pressure at the edge of the meniscus [Fig. 1(a)]. Subsequently, the air pressure in the chamber was increased using pressure drops ΔP of 20 to 1000 Pa causing the film to drain. Eventually the film becomes so thin that it ruptures. In the *thin* film, the pressure balance is [11]

$$P_i + \Delta P + \frac{2\sigma}{R_{bw}} = P_H(h,r) + P_\infty + \Pi_{\mathrm{vdW}}(h,r) + \frac{\sigma}{2r}\frac{\partial}{\partial r}\left(r\frac{\partial h}{\partial r}\right), \quad (2)$$

where the last term describes the pressure due to curvature differences. A nomenclature and a description of all pressures is given in the Supplemental Material [33]. A coalescence or breakup time t_c is defined as the time between the onset of film expansion and rupture [25]. At least five measurements were performed for each combination of pressure drop and polymer concentration. For the 5 wt % solution an extra pressure drop of 1600 Pa and 15 measurements for each ΔP were conducted. More information about the experimental protocol, the viscosities, and the surface tensions of the solutions, can be found in the Supplemental Material [33].

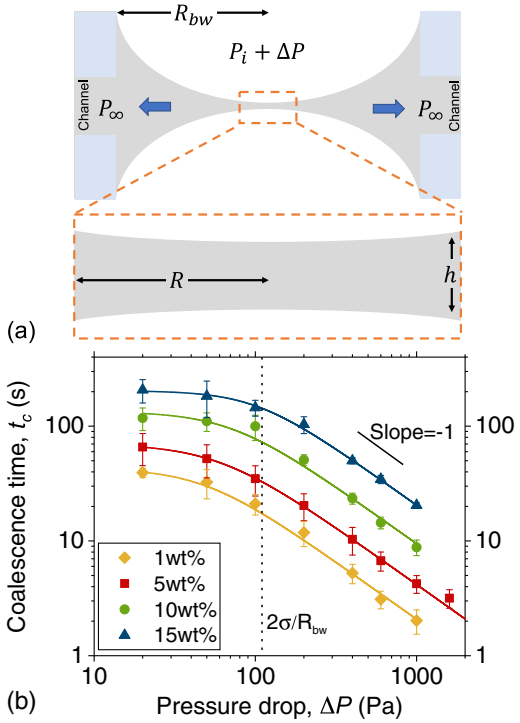

FIG. 1. Pressures and coalescence times. (a) Pressure contributions in our setup. (b) Evolution of the coalescence time with applied pressure drop for different polymer concentrations.

The experimental coalescence times t_c are shown in Fig. 1(b) for different ΔP. The same trends are observed for all polymer concentrations (with only different viscosities). For $\Delta P < 2\sigma/R_{bw}$, drainage is slow and there is no strong dependency on ΔP, indicative of a static film rupture caused by the fluctuations [20]. In this regime, capillary forces control coalescence [58]. For $\Delta P \gg 2\sigma/R_{bw}$, we cross over to a regime where the hydrodynamics dominate. Here, the t_c is inversely proportional to ΔP as predicted by Eq. (1). Because of the absence of surface active components, the mobility factors n^2 of all solutions were of $\mathcal{O}(10^{-2})$ (Supplemental Material [33]). Given the limitations of Eq. (1), the values of n are very approximative. However, the low surface stress carriage combined with long drainage times due to the high viscosity and the occurrence of osmotic effects [59], allowed at low ΔP the observation of the thickness fluctuations before rupture.

As the fluctuations are damped by capillarity they are expected to develop first in the flat rim of a dimpled film, where the small thickness ensures strong enough destabilizing vdW forces. Hence, fluctuations evolved in the θ direction [in the ring where film thickness is ≈30 nm, and the corresponding Π_{vdW} is $\mathcal{O}(10^2\mathrm{Pa})$], and not in the r direction, as usually assumed in axisymmetric models [20,60]. Images of a 15 wt% film at rupture ($\Delta P = 50$ Pa) and the corresponding thickness profiles of its rim are shown in Fig. 2. For $t \leq 190$ s, the film is draining and the rim's thickness is homogeneous. Differences of ≈1 nm that

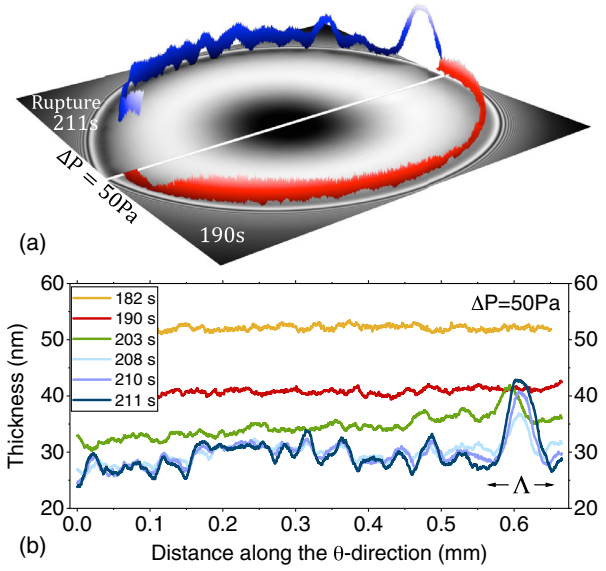

FIG. 2. Thickness fluctuations. (a) Interference images for a 15 wt% polymer film with the contour lines of the thickness profiles. (b) Thickness profiles at a constant distance from the contour of the film's rim. This initial distance Δr corresponds to the contour line where the maximum $\Delta h(\theta)$ is observed.

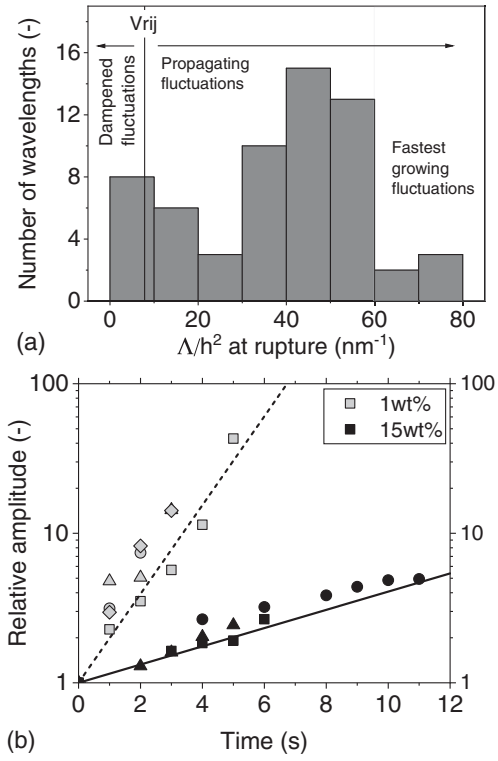

FIG. 3. Growth of fluctuations. (a) The distribution of measured Λ/h^2. The solid line denotes the prediction of Vrij for $\Lambda_{c,V}/h^2$. (b) The relative amplitude of the fluctuations $(h_{\max}-h)/(h_{\max}-h)_{t=0}$. Lines denote predictions for an average thickness of $h \approx 47$ nm.

are close to the lower limit of interferometry, can be attributed to noise and small errors in fitting a spline along the film's rim. At $t = 203$ s thickness fluctuations of $\Delta h \approx 5$ nm appear. Finally, from $t = 208$ s till rupture ($t = 211$ s), drainage is negligible and the average thickness at the rim remains constant at $h \approx 30$ nm. However, the amplitude of the fluctuations increases. The fluctuation spectra of the 1 wt% and 15 wt% films (with equal σ, A_H, and only different η) were similar, as hydrodynamics do not matter at rupture [8]. Vrij's analysis predicts both the critical wavelength below which fluctuations are damped, as well as the relative growth rate of the fastest fluctuations [Eq. (3)]. In our experiments, all observable Λ/h^2 (over all experiments and all times) were larger than the critical one [6] [Fig. 3(a)], with $\Lambda(h)$ being the distance between two consecutive minima [Fig. 2(b)]. The amplitude of fluctuations in nondraining films is expected to temporally increase as [9]

$$\frac{h_{\max}-h}{(h_{\max}-h)_{t=0}} = \exp\left(\frac{t}{\tau_{m,V}}\right), \tag{3}$$

where $h_{\max}$ is the maximum thickness of the fluctuation, t is the elapsed time after its first observation, and $\tau_{m,V} = 96\pi^2\sigma\eta_{\text{eff}}h^5A_H^{-2}$ is the characteristic time for its growth. An exponential fit describes the experimental evolution well with $h \approx 47$ nm. However, the good agreement with Vrij's model does not necessarily mean that the fluctuations are thermal in origin, nor that they are purely capillary in nature. Any perturbation of $\mathcal{O}(k_BT)$ (e.g., thermal, pressure, spatial variation of Π_{vdW}) with large enough wavelengths might cause propagating thickness fluctuations.

The situation changes when the applied ΔP increases. Vrij hinted to an interplay between hydrodynamics and capillary waves, suggesting that fluctuations must develop less for breakup to occur [6], predicting a *decrease* in h_c as ΔP increases. Both our experiments and literature results [26–31] show the opposite behavior. The increase in h_c can be rationalized by the combined effects of the increase in film radius and the damping of the fluctuations by the spatial variations of $P_H(r)$. By expressing the hydrodynamic stress by the capillary number, $\text{Ca} = \Delta P/(2\sigma/R_{bw})$, and conducting a local pressure balance (Supplemental Material [33]), we obtain the critical wavelength under the influence of hydrodynamic stresses $\Lambda_c = \Lambda_{c,V}(1+\text{Ca})$, where $\Lambda_{c,V}$ the critical wavelength for a quiescent film [6]. Similarly, the characteristic time for the evolution of fluctuations is $\tau_m = \tau_{m,V}(1+\text{Ca})^{-2}$. At high ΔP the film drains so fast down to its h_c, that the damped fluctuations do not fully develop to be detected within the resolution limit of interferometry. The growth of fluctuations leads to a rupture time $t_r(h) = f\tau_m(h)$, f being a prefactor equal to ≈ 6 [6] [Fig. 4(a)]. Given that t_r is stochastic, this corresponds to the most probable value, determined by the fastest growing fluctuation. The stochasticity can be

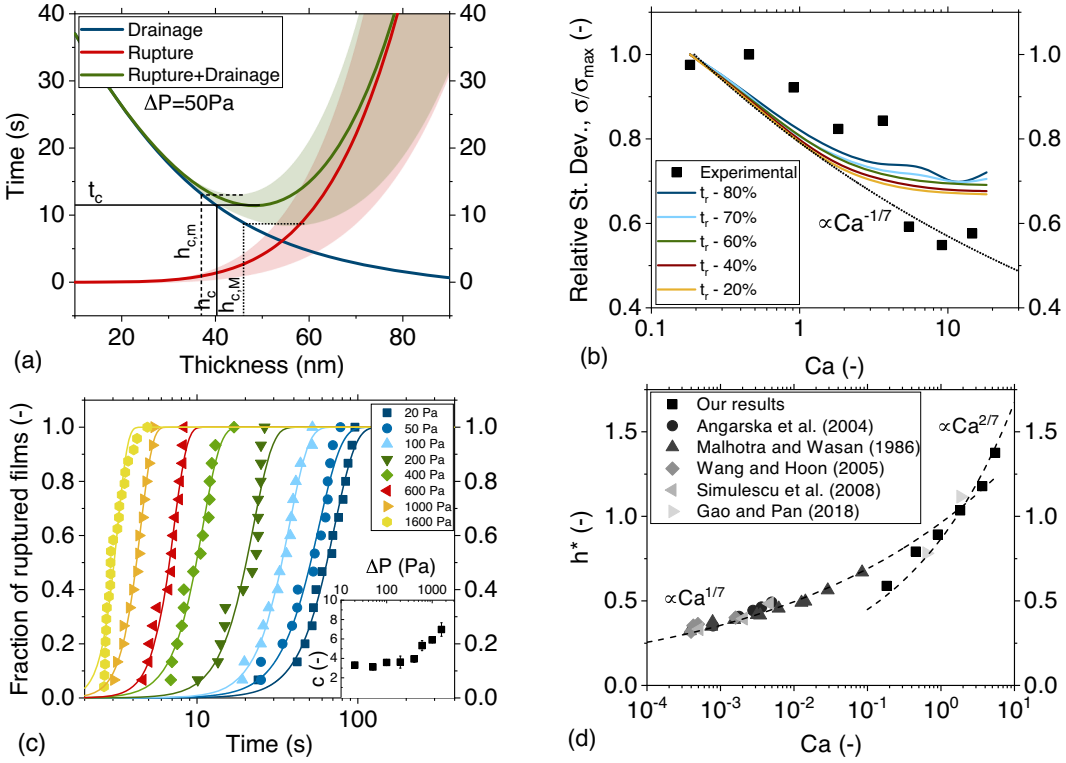

FIG. 4. Stochasticity of coalescence. (a) Determination of t_c following Ref. [6] for a film with the time-average experimental radius and the viscosity of the 5 wt% solution ($\Delta P = 50$ Pa). The 60% variance of t_r results in a distribution of t_c and h_c. (b) Experimental and predicted $\bar{\sigma}/\bar{\sigma}_{\max}$ as a function of Ca for different variances in t_r. (c) Cumulative distribution of t_c fitted with the Weibull function (5 wt% solution). The shape factor c is shown in the inset. (d) The dimensionless critical thickness of all solutions as a function of Ca plotted with literature results [26–31]. The error bars have been omitted for clarity, but are shown in the Supplemental Material [33].

included by considering a variance ($s\%$) of this t_r, conceptually shown as a red-shaded area in Fig. 4(a) ($s = 60\%$). The competing process has a hydrodynamic drainage time $t_d(h)$ roughly given by Eq. (1). Breakup is most probable at the minimum of $t_d(h) + t_r(h)$. The distribution of t_r causes a subsequent distribution of t_c, conceptually shown by the green area. Extrapolation of these minima to the t_d curves allows the determination of h_c. A distribution of critical thicknesses is expected, the minimum ($h_{c,m}$), maximum ($h_{c,M}$), and most probable (h_c) of which correspond to the slowest, fastest, and most probable coalescence times, respectively. In our analysis, the determined t_r and t_d are only approximative, given the assumptions involved in obtaining both equations, and any discussion is limited to a semiquantitative level.

Regardless of the detailed hydrodynamic model used, it is expected that as ΔP increases, drainage proceeds faster, while rupture decelerates and fluctuations are damped. This results in a reduction of the stochastic character of coalescence, reflected in the standard deviation, $\bar{\sigma}$, of t_c. The predicted relative $\bar{\sigma}$ for rupture times with different variances is plotted as a function of Ca in Fig. 4(b), along with experimental values for the 5 wt% films. In all cases, $\bar{\sigma}$ decreases with increasing Ca, in line with earlier studies [18,20,61–63]. In experiments, coalescence appears as deterministic when $\bar{\sigma}$ is lower than the experimental noise ($\simeq 18\%$ in our experiments). The differences observed between predicted and experimental $\bar{\sigma}$ at high Ca are most likely due to the assumptions involved in Eq. (1), i.e., flat films of constant radius. If the t_c are plotted as cumulative distributions and fitted with a Weibull function, then their spread narrows as Ca increases [Fig. 4(c)]. The shape factor of the distribution c was found to increase as $c \propto (1 + \mathrm{Ca})^{2/7}$ [inset of Fig. 4(c) and Supplemental Material [33]]. A quantitative prediction of the changes in $\bar{\sigma}$ and c is only possible through detailed numerical simulations which include the interplay between capillarity and hydrodynamics [1] yet furthermore also account for the random evolution of propagating fluctuations.

The critical thickness also depends on Ca. Solving $dt_d(h)/dh + dt_r(h)/dh = 0$ with respect to h_c results in

$$h_c = h_{c,V}(1 + \mathrm{Ca})^{2/7}, \tag{4}$$

where $h_{c,V} \simeq 0.268(A_H^2 R^2 P_{\mathrm{tot}}^{-1} f^{-1} \sigma^{-1})^{1/7}$ is Vrij's result [6], with the generalization that all pressure contributions (P_{tot}) must be considered at rupture. For high P_H, the extra pressure due to the evolution of fluctuations is negligible, and Eq. (4) is equivalent to a local pressure balance, similar to the one proposed by Leal *et al.* [64,65] for deterministic

rupture. The dimensionless critical thickness $h^* = h_c/h_{c,V}$ is shown as function of Ca in Fig. 4(d), together with results from earlier studies [26–31]. Good agreement with Eq. (4) is observed. For $\mathrm{Ca} < 1$, there is a weak dependence of $h^* \propto \mathrm{Ca}^{1/7}$, following the effect of film expansion on h_c. Further increasing Ca causes a more pronounced hydrodynamic damping and a gradual transition to a $h^* \propto \mathrm{Ca}^{2/7}$ scaling (Supplemental Material [33]).

Similarly, effects that accelerate drainage, such as changes in the stress-boundary conditions [66] and instabilities [67], are expected to promote determinism as they will decrease the absolute values of $\bar{\sigma}$. Although in films with surface stresses fluctuations are damped [68,69], dust contamination [70] or surface concentration fluctuations [71] are expected to act in a way similar to the randomly evolving capillary waves. Evidently, detailed numerical simulations that account both for changes in the stress-boundary conditions and for the random evolution of propagating fluctuations are essential in precisely quantifying the reduction in the stochastic character of coalescence and in exactly defining the regimes that this change takes place.

In this Letter the competition between the characteristic timescales of drainage and rupture has been experimentally determined. Our experimental results rationalize previous disagreements in literature about the stochastic versus deterministic nature of coalescence. Both characters can manifest themselves, depending on the relative importance of hydrodynamic and capillary stresses, as described by the capillary number Ca.

The authors would like to thank Professor E. Dufresne (ETH Zürich) for stimulating comments and the ETH Energy Science Center Partnership with Shell for the financial support.

*Corresponding author.
jan.vermant@mat.ethz.ch

[1] D. Y. Chan, E. Klaseboer, and R. Manica, Soft Matter **7**, 2235 (2011).
[2] O. Reynolds, Phil. Trans. R. Soc. London **177**, 157 (1886).
[3] S. Jeelani and S. Hartland, J. Colloid Interface Sci. **164**, 296 (1994).
[4] A. Scheludko, Proc. Konikl. Ned. Akad. Wet. B **65**, 86 (1962).
[5] A. Sheludko, Adv. Colloid Interface Sci. **1**, 391 (1967).
[6] A. Vrij, Discuss. Faraday Soc. **42**, 23 (1966).
[7] B. P. Radoev, A. D. Scheludko, and E. D. Manev, J. Colloid Interface Sci. **95**, 254 (1983).
[8] D. G. Aarts, M. Schmidt, and H. N. Lekkerkerker, Science **304**, 847 (2004).
[9] A. Vrij and J. T. G. Overbeek, J. Am. Chem. Soc. **90**, 3074 (1968).
[10] I. Ivanov, B. Radoev, E. Manev, and A. Scheludko, Trans. Faraday Soc. **66**, 1262 (1970).
[11] D. S. Valkovska, K. D. Danov, and I. B. Ivanov, Adv. Colloid Interface Sci. **96**, 101 (2002).
[12] E. Rio and A.-L. Biance, Chem. Phys. Chem **15**, 3692 (2014).
[13] E. Forel, B. Dollet, D. Langevin, and E. Rio, Phys. Rev. Lett. **122**, 088002 (2019).
[14] S. Perumanath, M. K. Borg, M. V. Chubynsky, J. E. Sprittles, and J. M. Reese, Phys. Rev. Lett. **122**, 104501 (2019).
[15] V. C. Suja, A. Kar, W. Cates, S. Remmert, P. Savage, and G. Fuller, Proc. Natl. Acad. Sci. U.S.A. **115**, 7919 (2018).
[16] I. U. Vakarelski, R. Manica, X. Tang, S. J. OShea, G. W. Stevens, F. Grieser, R. R. Dagastine, and D. Y. Chan, Proc. Natl. Acad. Sci. U.S.A. **107**, 11177 (2010).
[17] I. U. Vakarelski, R. Manica, E. Q. Li, E. S. Basheva, D. Y. Chan, and S. T. Thoroddsen, Langmuir **34**, 2096 (2018).
[18] Y. Vitry, S. Dorbolo, J. Vermant, and B. Scheid, Adv. Colloid Interface Sci. **270**, 73 (2019).
[19] J. L. Joye, G. J. Hirasaki, and C. A. Miller, Langmuir **8**, 3083 (1992).
[20] M. S. Shah, V. van Steijn, C. R. Kleijn, and M. T. Kreutzer, J. Fluid Mech. **876**, 1090 (2019).
[21] V. V. Yaminsky, S. Ohnishi, E. A. Vogler, and R. G. Horn, Langmuir **26**, 8061 (2010).
[22] P. J. Janssen and P. D. Anderson, Macromol. Mater. Eng. **296**, 238 (2011).
[23] B. Liu, R. Manica, Q. Liu, E. Klaseboer, Z. Xu, and G. Xie, Phys. Rev. Lett. **122**, 194501 (2019).
[24] N. Politova, S. Tcholakova, and N. Denkov, Colloids Surf. A Physicochem. Eng. Aspects **522**, 608 (2017).
[25] A. Kannan, I. C. Shieh, D. L. Leiske, and G. G. Fuller, Langmuir **34**, 630 (2018).
[26] J. Angarska, B. Dimitrova, K. Danov, P. Kralchevsky, K. Ananthapadmanabhan, and A. Lips, Langmuir **20**, 1799 (2004).
[27] A. Malhotra and D. Wasan, Chem. Eng. Commun. **48**, 35 (1986).
[28] L. Wang and R.-H. Yoon, Colloids Surf. A Physicochem. Eng. Aspects **263**, 267 (2005).
[29] V. Simulescu, J. Angarska, and E. Manev, Colloids Surf. A Physicochem. Eng. Aspects **319**, 21 (2008).
[30] D. S. Ivanova and J. K. Angarska, Colloids Surf. A Physicochem. Eng. Aspects **438**, 93 (2013).
[31] Y. Gao and L. Pan, Langmuir **34**, 14215 (2018).
[32] L. Cascão-Pereira, C. Johansson, H. Blanch, and C. Radke, Colloids Surf. A Physicochem. Eng. Aspects **186**, 103 (2001).
[33] See Supplemental Material at http://link.aps.org/supplemental/10.1103/PhysRevLett.125.158001 for more details on the experimental setup, other properties of the polymer solutions, and a comparison with other rupture models, which includes Refs. [34–57].
[34] P. J. Beltramo, R. Van Hooghten, and J. Vermant, Soft Matter **12**, 4324 (2016).
[35] T. M. Aminabhavi and G. Bindu, J. Chem. Eng. Data **39**, 529 (1994).
[36] A. Chesters, Chem. Eng. Res. Des. **69**, 259 (1991).
[37] F. Baldessari and L. G. Leal, Phys. Fluids **18**, 013602 (2006).
[38] P. Janssen, P. Anderson, G. Peters, and H. Meijer, J. Fluid Mech. **567**, 65 (2006).

[39] D. Y. Chan, E. Klaseboer, and R. Manica, Soft Matter **6**, 1809 (2010).
[40] P. Bataille and D. Patterson, J. Polym. Sci. A Gen. Papers **1**, 3265 (1963).
[41] *Oppanol B Technical Information* (BASF, Ludwigshafen, 2005).
[42] E. Lifshitz, J. Exp. Theor. Phys. USSR **29**, 83 (1955).
[43] J. N. Israelachvili, *Intermolecular and Surface Forces* (Academic Press, New York, 2011).
[44] S. Dorbolo, D. Terwagne, R. Delhalle, J. Dujardin, N. Huet, N. Vandewalle, and N. Denkov, Colloids Surf A Physicochem. Eng. Aspects **365**, 43 (2010).
[45] V. C. Suja, A. Kar, W. Cates, S. Remmert, and G. Fuller, J. Colloid Interface Sci. **567**, 1 (2020).
[46] H. Rinne, *The Weibull Distribution: A Handbook* (Chapman and Hall/CRC, London, 2008).
[47] C. Lu, R. Danzer, and F. D. Fischer, Phys. Rev. E **65**, 067102 (2002).
[48] R. Doremus, J. Appl. Phys. **54**, 193 (1983).
[49] B. Toshev and I. Ivanov, Colloid Polym. Sci. **253**, 558 (1975).
[50] S. Karakashev, Colloids Surf. A Physicochem. Eng. Aspects **372**, 151 (2010).
[51] E. D. Manev and A. V. Nguyen, Adv. Colloid Interface Sci. **114**, 133 (2005).
[52] C. Stubenrauch, D. Langevin, D. Exerowa, E. Manev, P. M. Claesson, L. B. Boinovich, and R. v. Klitzing, Langmuir **23**, 12457 (2007).
[53] P. A. Kralchevsky, K. D. Danov, and J. K. Angarska, Langmuir **24**, 2953 (2008).
[54] R.-H. Yoon and L. Wang, Langmuir **24**, 5194 (2008).
[55] G. P. Dubey and M. Sharma, J. Chem. Eng. Data **53**, 1032 (2008).
[56] B. Coursey and E. L. Heric, J. Chem. Eng. Data **14**, 426 (1969).
[57] G. Hahn, P. Svejda, and A. Dallos, Fluid Phase Equilib. **86**, 293 (1993).
[58] H. Yang, C. C. Park, Y. T. Hu, and L. G. Leal, Phys. Fluids **13**, 1087 (2001).
[59] A. Nikolov and D. T. Wasan, Langmuir **8**, 2985 (1992).
[60] A. Sharma and E. Ruckenstein, Langmuir **3**, 760 (1987).
[61] G. E. Charles and S. G. Mason, J. Colloid Sci. **15**, 236 (1960).
[62] J. M. Frostad, A. Paul, and L. G. Leal, Phys. Rev. Fluids **1**, 033904 (2016).
[63] M. Dudek, D. Fernandes, E. H. Herø, and G. Øye, Colloids Surf. A Physicochem. Eng. Aspects **586**, 124265 (2020).
[64] Y. Yoon, F. Baldessari, H. D. Ceniceros, and L. G. Leal, Phys. Fluids **19**, 102102 (2007).
[65] A. S. Hsu, A. Roy, and L. G. Leal, J. Rheol. **52**, 1291 (2008).
[66] E. Hermans, M. S. Bhamla, P. Kao, G. G. Fuller, and J. Vermant, Soft Matter **11**, 8048 (2015).
[67] J.-L. Joye, G. J. Hirasaki, and C. A. Miller, Langmuir **10**, 3174 (1994).
[68] V. Bergeron, Langmuir **13**, 3474 (1997).
[69] E. Ruckenstein and R. K. Jain, J. Chem. Soc., Faraday Trans. 2 **70**, 132 (1974).
[70] P.-G. de Gennes, Chem. Eng. Sci. **56**, 5449 (2001).
[71] D. Exerowa, D. Kashchiev, and D. Platikanov, Adv. Colloid Interface Sci. **40**, 201 (1992).